Data in Brief 30 (2020) 105411

Contents lists available at ScienceDirect

Data in Brief

journal homepage: www.elsevier.com/locate/dib

Data Article

Design of defected TaN supercells dataset for structural and elastic properties from ab initio simulations and comparison to experimental data

Chen-Hui Li [a,*], Grégory Abadias [b], Laurent Belliard [c], Qing Miao Hu [d], Nicolas Greneche [a], Philippe Djemia [a,*]

[a] Laboratoire des Sciences des Procédés et des Matériaux, UPR 3407 CNRS, Université Sorbonne Paris Nord, Alliance Sorbonne-Paris-Cité, 99 Avenue J.B. Clément 93430 Villetaneuse, France
[b] Institut Pprime, UPR 3346, CNRS-Université de Poitiers-ENSMA, 11 Boulevard Marie et Pierre Curie, TSA 41123, Poitiers Cedex 9, F86073, France
[c] Sorbonne Université, CNRS, UMR 7588, Institut des NanoSciences de Paris, 4 Place Jussieu, Paris Cedex 05 75252, France
[d] Institute of Metal Research, Chinese Academy of Sciences, Wenhua Road 72, Shenyang 110016, PR China

ARTICLE INFO

Article history:
Received 8 November 2019
Revised 22 February 2020
Accepted 4 March 2020
Available online 11 March 2020

Keywords:
Thin films
Transition metal nitrides
Vacancies
Sound velocities
Elastic constants
Phonons
Supercells

ABSTRACT

These data are supplied for supporting their interpretations and discussions provided in the research article "Large influence of vacancies on the elastic constants of cubic epitaxial tantalum nitride layers grown by reactive magnetron sputtering" by Abadias et al. (2020) [doi: 10.1016/j.actamat.2019.11.041]. The datasheet describes the experimental methods used to measure the longitudinal (V_L) and transverse (V_T) sound velocities of cubic epitaxial TaN/MgO thin films, and their related cubic elastic constants (c_{11}, c_{12} and c_{44}), by the picosecond laser ultrasonic (PLU) and the Brillouin light scattering (BLS) techniques, respectively. First-principles numerical simulations provide additional data using specifically designed supercells of TaN structures, generated either by hand or using the alloy theoretical automated toolkit (ATAT) method [A. Zunger et al. (1990)], with different configurations (random, cluster and ordered) of defects (Ta and N vacancies). Phonons

* Corresponding authors.
E-mail addresses: lichcn1@outlook.com (C.-H. Li), djemia@univ-paris13.fr (P. Djemia).

https://doi.org/10.1016/j.dib.2020.105411

calculations support discussion of dynamical mechanical stability of defected TaN cubic structures. The data illustrate the huge role of vacancies in elastic properties and phase stability of TaN films.

Specifications table

Subject	Materials Science
Specific subject area	Elastic properties of transition metal nitrides
Type of data	Tables, Images, Figures POSCAR files of each supercells
How data were acquired	PLU and BLS techniques [3] measured V_L and V_T sound velocities, respectively. Related elastic constants (c) are obtained through $c = \rho V^2$, ρ being the mass density of the film measured by x-ray reflectivity [1]. Special quasi-random structures (SQS) supercells that mimic the random positions of Ta and N vacancies are generated by a Monte Carlo method implemented in ATAT [2] software. Other $2 \times 2 \times 2$ supercells of the conventional unit cell with different distribution of vacancies were made by hand while fully ordered structures were obtained by cluster expansion (CE) method. Density functional theory (DFT) calculations were performed using VASP code [4], and CE method was implemented in UNCLE [5] program. Phonon dispersion properties were calculated by the PHONOPY code [6] within the harmonic approximation, with the force constants obtained from density functional perturbation theory (DFPT) calculations implemented in VASP.
Data format	Raw, analyzed
Parameters for data collection	PLU and BLS measurements performed at room temperature (20 °C). A Sandercock-type 3 + 3 pass tandem Fabry-Perot interferometer, in the back-scattering geometry, was used for BLS experiments. The angle of incidence of light was varied from 30° to 80° A pump-probe technique employing a mode-locked Ti:Sapphire laser source operated at 800 nm with a repetition rate around 79.3 MHz was used for PLU measurements. DFT calculations were performed employing the plane-wave basis projector augmented wave method. A plane-wave energy cutoff of 520 eV and an energy convergence criteria of 10^{-8} eV were used. The k spacing in the reciprocal space was below 0.2 $Å^{-1}$. The generalized gradient approximation (GGA) with a Perdew-Burke-Ernzerhof exchange and correlation functional was employed for DFT calculations.
Description of data collection	Each BLS spectrum was fitted by a numerical model accounting for the vertical dynamical corrugation of the free surface [7]. Time of flight (TOF) between at least two echoes was used for $V_L = 2h / TOF$ by PLU. Thicknesses (h) of TaN thin films were carefully measured by x-ray reflectivity [1]. Structural parameters and elastic constants from defected structures with various defect concentrations and configurations are derived from DFT calculations.
Data source location	LSPM-CNRS, Université Sorbonne Paris Nord, Villetaneuse, France; PPRIME Institute, University of Poitiers, France
Data accessibility	With the article and on a public repository (for POSCAR files) Repository name: Mendeley data Data identification number: doi:10.17632/pvpd7ftfp6.1 Direct URL to data: http://dx.doi.org/10.17632/pvpd7ftfp6.1
Related research article	[1] G. Abadias, C–H. Li, L. Belliard, Q–M. Hu, N. Greneche, P. Djemia, Large influence of vacancies on the elastic constants of cubic epitaxial tantalum nitride layers grown by reactive magnetron sputtering, Acta Materia 184 (2020) 254–266

Value of the Data

- Experimental data illustrate the quality of the signal we analysed for sound velocities data assessment of TaN layers, while the designed supercells are useful to implement vacancy-type defects in TaN structures to evaluate their impact on the phase stability and elastic properties.
- These data can be used by any experimentalist colleagues who are working with picosecond laser ultrasonic and Brillouin light scattering techniques, and theoreticians performing ab initio simulations of disordered alloys properties.
- These data alleviate other researchers from performing the large number of computationally intensive DFT calculations required to compute the effects of vacancies on elastic properties of TaN or other related compounds with Ta or N vacancies.
- These data can be directly incorporated into mesoscale methods used in integrated computational materials engineering (ICME) of transition metal nitrides, including phase field simulations to predict the phase stability and morphological evolutions.

1. Data description

The relative change of the transient reflectivity, $\Delta r/r_0$, measured by PLU on TaN/MgO films is shown in Fig. 1 for the different orientations. One typical BLS spectrum measured on the $Ta_{0.93}N/MgO(001)$ sample ($h = 154$ nm) at an angle of incidence $\theta = 70°$ is displayed in Fig. 2. The experimental sound velocities (V_L, V_R and V_T) and the related elastic constants (c_L and c_T) obtained for the different TaN epitaxial films are summarized in Table 1. Data from DFT calculations of the formation energy, structural and elastic properties of mononitride TaN compounds with cubic NaCl-type ($Fm\bar{3}m$), NbO-type ($Pm\bar{3}m$) and tetragonal (P4/nmm) structures are reported in Tables 2 and 3. Data of CE calculations using the UNCLE program, for several over- and under-stochiometric ordered TaN compounds, are shown in Fig. 3. Their structural and elas-

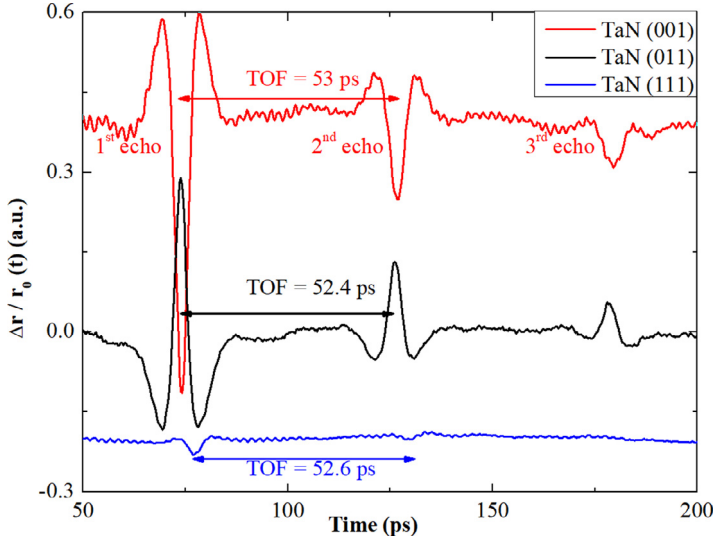

Fig. 1. Transient reflectivity change of δ-TaN-(001), -(011) and -(111) epitaxial films. From the time of flight (TOF), the film thickness (h) and the mass density (ρ), one can measure selectively $c_{11} = 530$ GPa, $(c_{11}+c_{12}+2c_{44})/2 = 502$ GPa and $(c_{11}+2c_{12}+4c_{44})/3 = 498$ GPa, respectively.

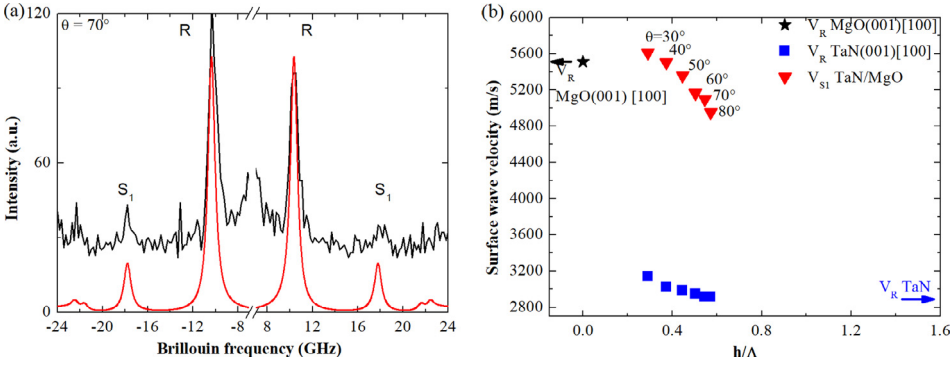

Fig. 2. (a) One typical BLS spectrum measured on the $Ta_{0.93}N$/MgO(001) sample ($h = 154$ nm) at an angle of incidence $\theta = 70°$ The fit of the spectrum considering the ripple mechanism at the free surface is also provided at the bottom (red line). R and S_1 denote the Rayleigh surface wave and the first Sezawa wave, respectively. (b) The sound wave velocity dispersion of R and S_1 as a function of the film thickness (h) over the acoustic wavelength (Λ) ratio h/Λ. Fitting parameters are $c_{44} = 137 \pm 3$ GPa and $c_{12} = 130 \pm 5$ GPa, considering $c_{11} = 530$ GPa fixed to the PLU measured value (For interpretation of the references to color in this figure legend, the reader is referred to the web version of this article.).

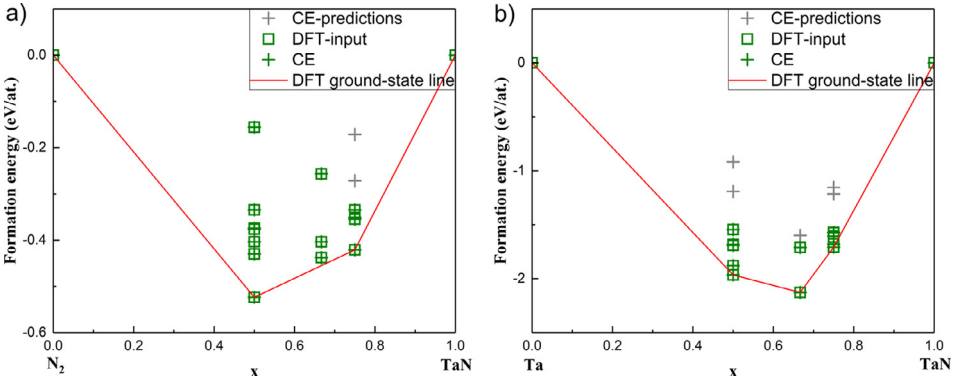

Fig. 3. (a) Formation energy of over-stoichiometric Ta_xN ($x \leq 1$) and (b) under-stoichiometric TaN_x ($x \leq 1$) structures evaluated by the CE method. The red line is the ground state calculated by DFT. The superposition of the open green square and green cross symbols suggests a good fitting of CE parameters. The gray cross is the predicted energy of several randomly generated structures according to the fitted CE model. Note that the CE calculations are used to provide some additional configurations with ordering vacancies in this work, to compare to the data from disordered SQS (For interpretation of the references to color in this figure legend, the reader is referred to the web version of this article.).

tic properties calculated by DFT are summarized in Table 4. The DFT formation energies of TaN and related compounds are summarized in Fig. 4. Atoms coordinates for several concentration of defects in supercells are provided in POSCAR data-files that can be dowloaded in *external Mendeley dataset* [8]. The dynamical lattice stability for $Fm\bar{3}m$ TaN (NaCl-structured), $Pm\bar{3}m$ TaN(NbO-structured), P4/nmm TaN, $Pm\bar{3}m$ Ta_3N_4 and $Pm\bar{3}m$ Ta_4N_3 are investigated by calculating their phonon dispersion relations. The phonon bands are depicted in Figs. 5–9.

2. Experimental design, materials, and methods

We first measured selectively with the picosecond laser ultrasonic (PLU) technique the longitudinal bulk sound wave velocity V_L and elastic constant c_L ($=\rho(V_L)^2$) of the δ-TaN epitaxial films with different crystal orientations: (001), (011) and (111). The relative change of the transient reflectivity, $\Delta r/r_0$, is shown in Fig. 1 for the different orientations. At least, two echoes are clearly visible for all the films.

Table 1
Experimental data of sound velocities and related elastic constant of TaN epitaxial films. $c_{12} = 130 \pm 5$ GPa was determined by fitting the first Sezawa surface acoustic wave (S_1) of the $Ta_{0.93}N$/MgO(001) sample. (*) denotes calculated values. Mass density from X-ray reflectivity (XRR) was used: $\rho_{XRR} = 15.6\,g/cm^3$.

Crystal orientation	V_L (m/s)	c_L (GPa) $\rho(V_L)^2$	V_R (m/s) along [100]	V_T (m/s) along [100]	c_T (GPa) $\rho(V_T)^2$	Poisson ratio $\nu = \frac{c_{12}}{(c_{11}+c_{12})}$
(001)	V_L [001] =5830	$c_{11} = 530$	2830	2963	$c_{44} = 137$	$\nu = 0.197$
	V_L [110] = 5471*	$B = (c_{11}+c_{12})/3 = 263$*				
	V_L [111] = 5347*	$(c_{11}+c_{12}+2c_{44})/2 = 467$*				
		$(c_{11}+2c_{12}+4c_{44})/3 = 446$*				
(011)	V_L [110] = 5656	$(c_{11}+c_{12}+2c_{44})/2 = 502$	–	–	–	
(111)	V_L [111] = 5635	$(c_{11}+2c_{12}+4c_{44})/3 = 498$	–	–	–	

Table 2
The calculated formation energy per TaN unit, lattice parameters, volume per TaN unit, elastic constants, effective Voigt-Reuss-Hill isotropic bulk modulus (B), shear elastic modulus (G), Young's modulus (E), Poisson's ratio (ν), and bulk/shear modulus ratio (B/G) of several mononitride TaN phases using the VASP code.

	$Fm\bar{3}m$ NaCl-type	$Pm\bar{3}m$ NbO-type	P4/nmm(I)	P4/nmm
E_{form}(eV/TaN)	−1.768 (−1.71[a], −1.75[d], −1.76[e])	−1.453	(−1.84[a])	−1.85 (−1.92[a,d])
a(Å)	4.426(4.420[a], 4.414[d], 4.427[e])	4.252	(3.076[a])	2.999 (2.967[a], 2.966[d])
c(Å)			(4.575[a])	4.874 (5.119[a], 5.099[d])
V(Å^3)	21.68 (21.59[a], 21.5[d], 21.69[e])	25.63	(21.65[a])	21.93 (22.54[a], 22.43[d])
c_{11}(GPa)	731.0 (732.3[a], 706.97[b], 817[c])	419.6	(663.3[a])	578 (727.0[a])
c_{12}(GPa)	121.5 (131.2[a], 155.7[b], 112[c])	206.4	(106.9[a])	283 (158.1[a])
c_{13}(GPa)			(290.3[a])	223 (149.9[a])
c_{33}(GPa)			(253.7[a])	262 (351.0[a])
c_{44}(GPa)	49.7 (70.9[a], 208.2[b], 71[c])	49.4	(105.3[a])	120 (211.1[a])
c_{66}(GPa)			(44.0[a])	294 (104.8[a])
B(GPa)	324.6 (331.6[a], 347[b])	277.5	(324.0[a])	297 (285.8[a])
G(GPa)	113.2 (132.5[a], 144[b])	67.6	(134.8[a])	136 (160.2[a])
E(GPa)	304.2 (350.7[a], 380[b])	187.5	(355.2[a])	353 (404.9[a])
ν (E/2G−1)	0.343 (0.324[a], 0.32[b])	0.387	(0.317[a])	0.3017 (0.264[a])
B/G	2.868 (2.503[a], 2.41[b])	4.105	(2.403[a])	2.183 (1.784[a])

[a] Hu et al. [9],
[b] Mota et al. [10],
[c] Zhao et al. [11],
[d] Kim et al. [12],
[e] Koutná et al. [13]

Table 3
The lattice parameters, Wyckoff positions, internal coordinates, and Ta-N distance in the Ta-N octahedra of the cubic δ-TaN compound ($Fm\bar{3}m$) and its corresponding values in the tetragonal TaN phase with P4/nmm symmetry.

	$Fm\bar{3}m$	P4/nmm
a (Å)	4.426(4.420[a])	2.999 (2.967[a])
c (Å)		5.119
Ta	4a (0, 0, 0)	2c (0, 1/2, z), z=0.776(0.727[a])
N	4b (1/2, 1/2, 1/2)	2c (0, 1/2, z), z=0.319(0.165[a])
d(Ta-N) (Å)	2.213 (2.210[a][6[b]])	2.169 (2.169[a][4[b]]), 2.243 (2.242[a][1[b]]), 2.880 (2.877[a][1[b]])

[a] Hu et al. [9],
[b] The number of Ta-N bonds with the given distance value around a Ta atom.

Table 4
The calculated formation energy per atom, lattice parameters, volume per Ta_xN_y unit, elastic constants, effective Voigt-Reuss-Hill isotropic bulk modulus (B), shear elastic modulus (G), Young's modulus (E), Poisson's ratio (ν), and bulk/shear modulus ratio (B/G) of several non-stoichiometric ordered Ta_xN_y phases, identified from CE calculations.

Space group Vac. conc. (N or Ta)	TaN Fm$\bar{3}$m 0/0	Ta_3N_4 I4/mmm 0.125 (Ta)	Ta_2N_3 Immm 0.17 (Ta)	TaN_2 I4$\bar{1}$/amd 0.25 (Ta)	Ta_4N_3 I4/mmm 0.125 (N)	Ta_2N I4$\bar{1}$/amd 0.25 (N)
E_{form}(eV/atom)	−0.884	−1.066	−1.062	−0.384	−0.938	−0.840
a(Å)	4.426	4.291	9.777	4.031	4.404	4.421
b(Å)			4.036			
c(Å)		8.589	3.081	9.939	8.619	8.201
V(Å^3)	21.68	79.09	60.80	40.39	83.58	40.08
c_{11}(GPa)	731	679	341	424	660	490
c_{12}(GPa)	121.5	167	263	158	107.5	142.5
c_{13}(GPa)		101	127	135	151	194
c_{22}(GPa)			484			
c_{23}(GPa)			157			
c_{33}(GPa)		667	451	187	606	413
c_{44}(GPa)	49.7	148	126	70	106	123
c_{55}(GPa)			70			
c_{66}(GPa)		131	80	21	134	136
B(GPa)	324.6	307	263.3	210.1	305	272.6
G(GPa)	113.2	320.4	97.4	60.7	158.3	132.6
E(GPa)	304.2	860.5	259.5	164.5	404.5	342.2
ν	0.343	0.343	0.331	0.356	0.277	0.290
B/G	2.868	0.958	2.702	3.463	1.926	2.056

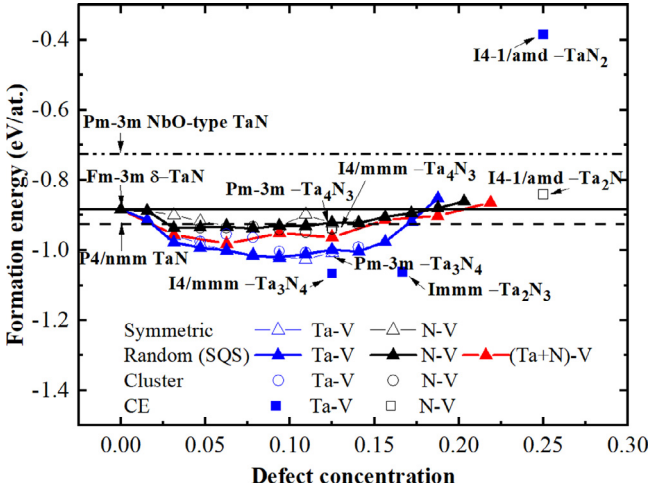

Fig. 4. The formation energy of cubic TaN and related compounds as a function of defect concentration. For defect-free TaN, 3 different phases were considered, namely, the Pm$\bar{3}$m NbO-type, Fm$\bar{3}$m cubic one and P4/nmm tetragonal one. The influence of Ta, N vacancies or both (Schottky) was evaluated. Considering different organizations of vacancies, 3 different types of defected structures were employed, i.e., "symmetric", "random" and "cluster". Details can be found in Ref. [1]. Additional data of the formation energy of some ordered structures generated from CE were also provided as a comparison to other structures.

Considering the value of 530 GPa for the c_{11} elastic constant as obtained from the $Ta_{0.93}N$/MgO(001) film by PLU, the other elastic constants, c_{44} and c_{12}, could be determined by the Brillouin light scattering (BLS) technique. c_{44} is found to be mostly dependent on the Rayleigh surface wave (R), while c_{12} is related to the first Sezawa wave (S_1), see Fig. 2a. c_{44} and c_{12} were extracted from the sound velocity dispersion curve for different angles of incidence θ

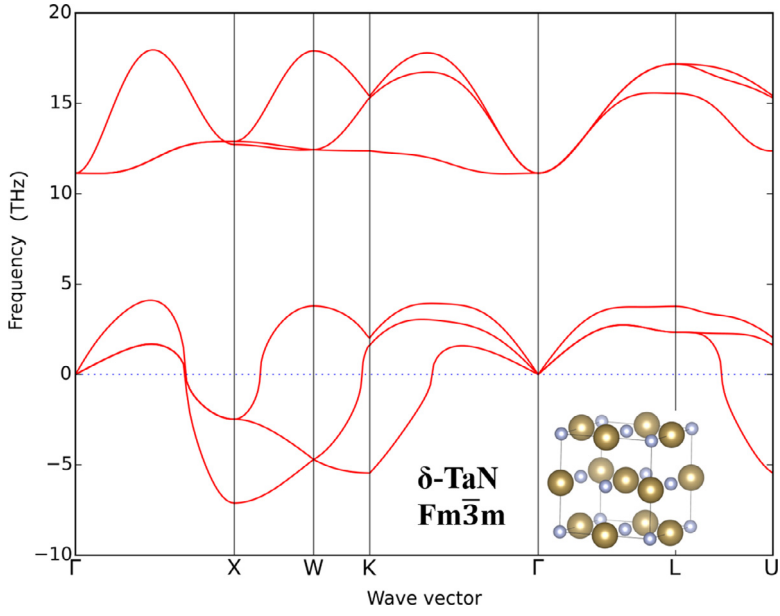

Fig. 5. The phonon dispersion curves of δ-TaN compound (Fm$\bar{3}$m symmetry).

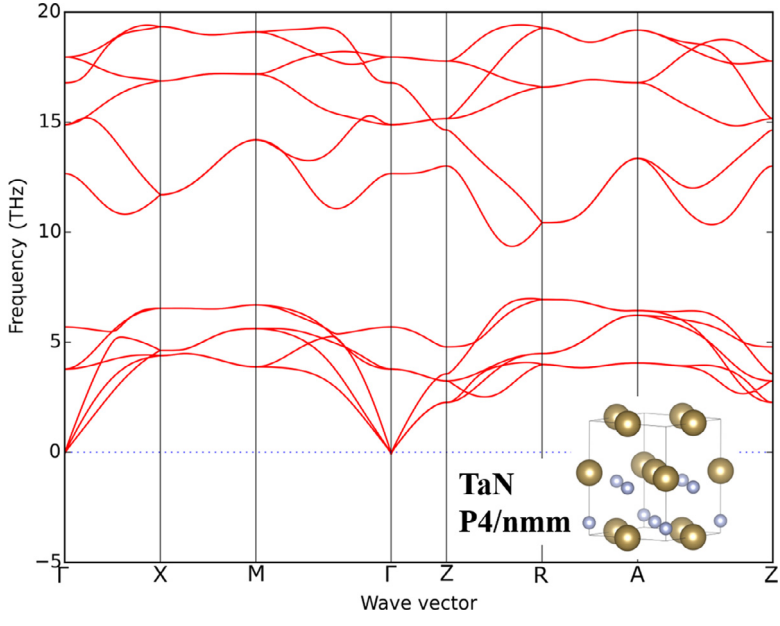

Fig. 6. The phonon dispersion curves of tetragonal TaN compound with P4/nmm symmetry.

(30–80°), see Fig. 2b, by fitting each BLS spectrum considering the ripple mechanism at the free surface [7].

The experimental data for sound velocities (V_L, V_R and V_T) and the related elastic constants (c_L and c_T) obtained for the different TaN epitaxial films are summarized in Table 1.

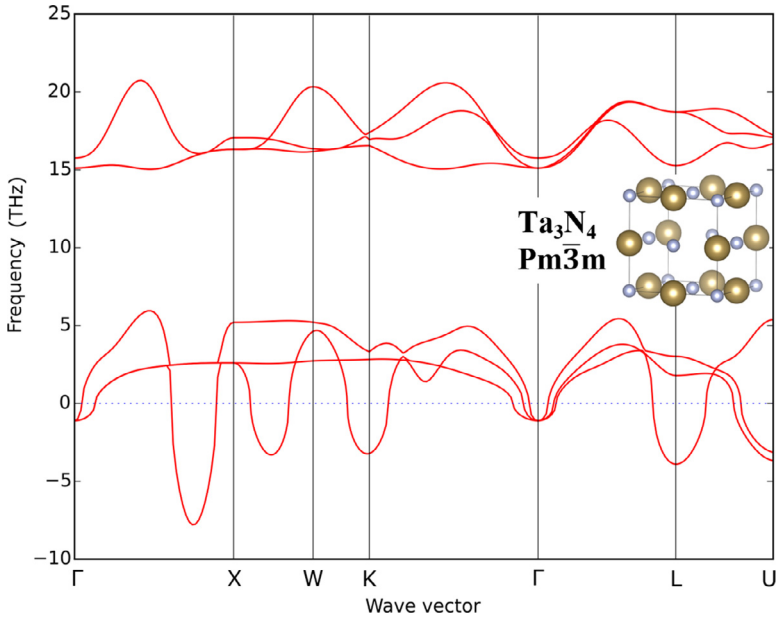

Fig. 7. The phonon dispersion curves of Ta_3N_4 compound with $Pm\bar{3}m$ symmetry.

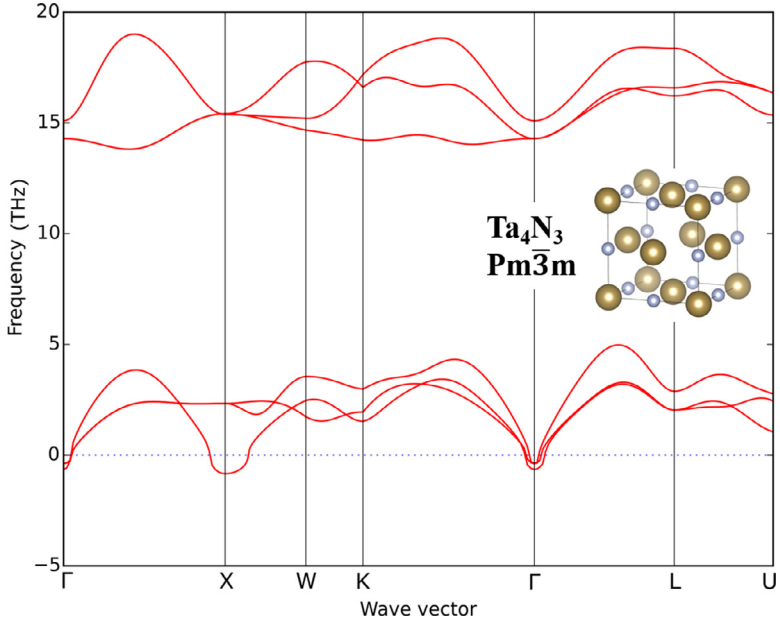

Fig. 8. The phonon dispersion curves of Ta_4N_3 compound with $Pm\bar{3}m$ symmetry.

Density functional theory (DFT) calculations using the VASP code [4] of the formation energy, structural and elastic properties of mononitride TaN compounds with cubic NaCl-type ($Fm\bar{3}m$), NbO-type ($Pm\bar{3}m$) and tetragonal (P4/nmm) structures are reported in Tables 2 and 3. The particular case of the NbO-type structure simulates a cubic structure with 25 at. % Schottky defects (12.5 at. % Ta vacancy + 12.5 at. % N vacancy). The data computed by Hu et al. [9] for

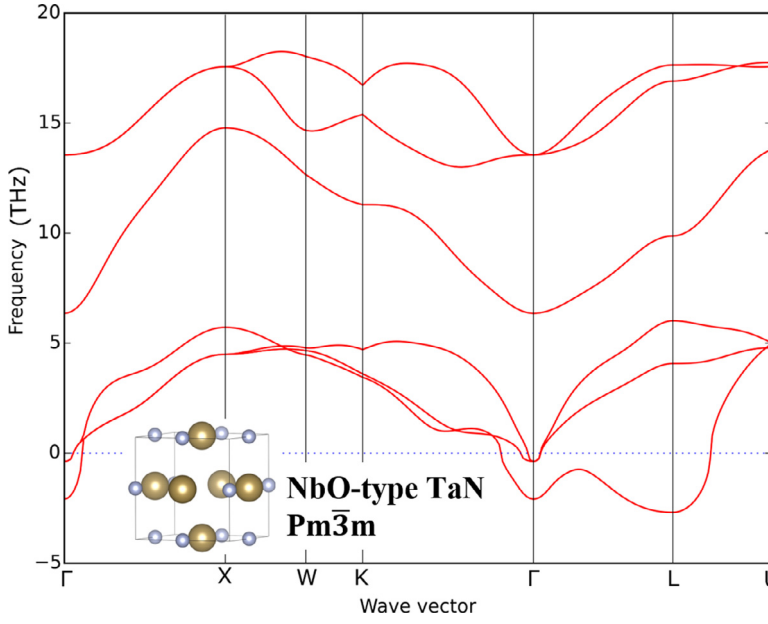

Fig. 9. The phonon dispersion curves of TaN compound with $Pm\bar{3}m$ symmetry.

the tetragonal P4/nmm(I) TaN structure are also reported. Data of cluster expansion (CE) calculations using the UNCLE program [5], for several over- and under-stochiometric ordered TaN compounds, are shown in Fig. 3. Their structural and elastic properties are summarized in Table 4.

The design of SQS supercells and atoms coordinates in supercells are described below and hyperlink to their external Mendeley dataset [8] is provided. Their POSCAR data-files defining different defects concentration can be downloaded. Hyperlink to the POSCAR data-files of Ta_xN_y supercells with "random" SQS configuration of vacancies and "Schottky defects" used in this work for DFT calculations. The design of SQS supercell by ATAT Monte Carlo method is explained in Ref. [2]. Hyperlink to the POSCAR data-files of Ta_xN_y supercells with "symmetric" configuration used in this work for DFT calculations. We considered ordered distribution of vacancies (denoted as "symmetric" configuration) by removing atoms with certain site symmetries from the $2 \times 2 \times 2$ supercell. Hence, in the symmetric configurations, all the defected structures remain cubic. The vacancies in "symmetric" configurations are not randomly distributed as in SQS. They are created in a symmetric manner referring to the 3-fold rotational symmetry along the [111] direction. The configurations are generated progressively by removing an atom from the $2 \times 2 \times 2$ supercell by one of the following manners, (*i*) 1 cubic center atom (1 V), (*ii*) *i*+ 1 vertex of the cubic (2 V), (*iii*) 3 face centers (3 V), (*iv*) *i*+*iii* (4 V), (*v*) +*ii*+*iii* (5 V), (*vi*) *iii*+ 3 edge centers (6 V), (*vii*) *vi*+*i* (7 V), (*vii*) *vi*+*ii* (8 V). Note that the structure has still cubic symmetry (equal in 3 directions) after vacancies creation for each step.

Hyperlink to the POSCAR data-files of Ta_xN_y supercells with "cluster" configuration used in this work for DFT calculations. In the case of cluster configurations, the vacancies are manually created by removing adjacent Ta or N atoms, respectively for clustered Ta or N vacancies. For example, a N(0) atom has 12 neighboring N(1–12) atoms, we first remove one N(0), then a neighboring N(1) of this first N(0), then a second neighboring N(2), … The vacancies form a cluster in such a way. It is the same methodology for Ta atoms.

Hyperlink to the POSCAR data-files of ordered Ta_xN_y compounds used in this work and obtained from CE method. "Perfectly ordered" structures were found by the CE method to have the lowest energies within the interested concentration range. Although they have higher symmetry

compared to SQS, it is better to name them specifically as "CE ground state (ordered) structures" to distinguish them from the symmetric ones that were generated manually.

The phonon dispersion properties of $Fm\bar{3}m$ TaN and related structures were calculated by PHONOPY code [6] within the harmonic approximation, using density functional perturbation theory (DFPT) calculations implemented in VASP. For the cubic phases, the calculations were performed with a $4 \times 4 \times 4$ supercell of the conventional unit cell, while for the tetragonal phase, a $5 \times 5 \times 3$ supercell was used, with each dimension of the supercells larger than 12 Å, in order to minimize the finite size effect. The $2 \times 2 \times 2$ Monkhorst-Pack *k*-point mesh was applied to both cubic and tetragonal phases, respectively, in the case of force constant calculations. An electronic energy convergence of 10^{-8} eV were adopted to ensure accurate force constant calculations.

CRediT authorship contribution statement

Chen-Hui Li: Writing - original draft, Conceptualization, Methodology, Investigation, Formal analysis, Visualization, Writing - review & editing. **Grégory Abadias:** Writing - original draft, Writing - review & editing, Resources, Investigation, Project administration, Funding acquisition, Supervision. **Laurent Belliard:** Investigation, Resources. **Qing Miao Hu:** Writing - review & editing. **Nicolas Greneche:** Resources. **Philippe Djemia:** Writing - original draft, Writing - review & editing, Resources, Investigation, Project administration, Funding acquisition.

Acknowledgments

This work has been performed within the M.ERA-NET project MC2 “Multi-scale Computational-driven design of novel hard nanostructured Coatings” and funded by the French ANR program (Project No. ANR-13-MERA-0002-02). C-H. Li acknowledge the support of CSC for his PhD funding. Q-M. Hu acknowledge the support of university Paris 13 for several visiting professor positions.

Conflict of Interest

The authors declare that they have no known competing financial interests or personal relationships which have, or could be perceived to have, influenced the work reported in this article.

Supplementary materials

Supplementary material associated with this article can be found, in the online version, at doi:10.1016/j.dib.2020.105411.

References

[1] G. Abadias, C-H. Li, L. Belliard, Q-M. Hu, N. Greneche, P. Djemia, Large influence of vacancies on the elastic constants of cubic epitaxial tantalum nitride layers grown by reactive magnetron sputtering, Acta Mater. 184 (2020) 254–266, doi:10.1016/j.actamat.2019.11.041.

[2] A. Zunger, S.-H. Wei, L.G. Ferreira, J.E. Bernard, Special quasirandom structures, Phys. Rev. Lett. 65 (1990) 353–356, doi:10.1103/PhysRevLett.65.353.

[3] G. Abadias, P. Djemia, L. Belliard, Alloying effects on the structure and elastic properties of hard coatings based on ternary transition metal (M=Ti, Zr or Ta) nitrides, Surf. Coatings Technol. 257 (2014) 129–137, doi:10.1016/j.surfcoat.2014.08.022.

[4] G. Kresse, J. Furthmüller, Efficient iterative schemes for ab initio total-energy calculations using a plane-wave basis set, Phys. Rev. B. 54 (1996) 11169–11186, doi:10.1016/0927-0256(96)00008-0.

[5] D. Lerch, O. Wieckhorst, G.L.W. Hart, R.W. Forcade, S. Müller, UNCLE: A code for constructing cluster expansions for arbitrary lattices with minimal user-input, Model. Simul. Mater. Sci. Eng. 17 (2009) 055003, doi:10.1088/0965-0393/17/5/055003.

[6] A. Togo, I. Tanaka, First principles phonon calculations in materials science, Scr. Mater. 108 (2015) 1–5, doi:10.1016/J.SCRIPTAMAT.2015.07.021.
[7] R. Loudon, Theory of Surface-Ripple Brillouin Scattering by Solids, Phys. Rev. Lett. 40 (1978) 581–583, doi:10.1103/PhysRevLett.40.581.
[8] C-H. Li, P. Djemia, G. Abadias, Design of defected TaN supercells dataset, Mendeley Data (2019), doi:10.17632/pvpd7ftfp6.1.
[9] S. Hu, C. Xu, Y. Lao, Y. Wang, H. Zhang, G.J. Zhang, J. Yang, The stabilization of the rocksalt structured tantalum nitride, J. Appl. Phys. 122 (2017) 045109, doi:10.1063/1.4989415.
[10] O.U.O. Mota, R.A. Araujo, H. Wang, T. Çağın, Mechanical properties of metal nitrides for radiation resistant coating applications: a DFT study, Phys. Proced. 66 (2015) 576–585, doi:10.1016/J.PHPRO.2015.05.077.
[11] E. Zhao, B. Hong, J. Meng, Z. Wu, First principles investigation on the ultra-incompressible and hard TaN, J. Comput. Chem. 30 (2009) 2358–2363, doi:10.1002/jcc.21234.
[12] T.E. Kim, S. Han, W. joon Son, E. Cho, H.S. Ahn, S. Shin, Phase stability and electronic structures of stoichiometric tantalum mononitrides, Comput. Mater. Sci. 44 (2008) 577–580, doi:10.1016/j.commatsci.2008.04.017.
[13] N. Koutná, D. Holec, O. Svoboda, F.F. Klimashin, P.H. Mayrhofer, Point defects stabilise cubic Mo-N and Ta-N, J. Phys. D. Appl. Phys. 49 (2016) 375303, doi:10.1088/0022-3727/49/37/375303.